PHYSICAL REVIEW E **86**, 030702(R) (2012)

Defect coalescence in spherical nematic shells

Teresa Lopez-Leon,[1,*] Martin A. Bates,[2] and Alberto Fernandez-Nieves[1]
[1]*School of Physics, Georgia Institute of Technology, Atlanta, Georgia 30332, USA*
[2]*Department of Chemistry, University of York, York YO10 5DD, United Kingdom*
(Received 7 May 2012; published 28 September 2012)

We study coalescence of topological defects in nematic liquid crystals confined to spherical shells using both experiments and computer simulations. We observe that the four $s = +\frac{1}{2}$ defects that are present due to topological constraints imposed by the spherical geometry coalesce by pairs after changing the molecular orientation at the outer surface from tangential to perpendicular; the result is the formation of two single $s = +1$ defects. It is noteworthy that the speed of the coalescence process is peaked when the defects are at opposite points on the equator of the shell; this maximum results from the thickness inhomogeneity of the shells.

DOI: 10.1103/PhysRevE.86.030702 PACS number(s): 61.30.Jf, 61.30.Hn, 83.80.Xz

Defects are spatial regions where the characteristic order of a material is disrupted. Their presence determines to a large extent the physical properties of the material. As a result, understanding their behavior and interactions is crucial and could enable precise control of material properties. Nematic liquid crystal droplets exemplify this fact very well, for example, in their response to electric fields. Nematics typically consist of rodlike molecules aligned, on average, along a common axis or director, **n**; they thus posses orientational order. When confined to the spherical volume of a droplet, the presence of defects, which are regions where **n** is undefined, is unavoidable; this directly results from the topological characteristics of the sphere. These defects can be points or lines depending on the boundary conditions for **n** at the confining surface and cannot be removed; they are thus topological defects and are present even in the ground state of the system [1].

Defects in nematic liquid crystals are characterized by their topological strength, s, which is a semi-integer number indicating how much **n** rotates along a path encircling the defect. This topological strength is also called topological charge to emphasize that interactions between defects, as those between electrical charges, can either be repulsive or attractive. In fact, the interaction energy per unit length of two defects with topological charge s_1 and s_2 separated by a distance r is [2]

$$W_{12} = \pi K (s_1 + s_2)^2 \ln \frac{R}{r_c} - 2\pi K s_1 s_2 \ln \frac{r}{2r_c}, \qquad (1)$$

with R the system size, K the Frank elastic constant of the nematic, and r_c the radius of the defect core. This expression assumes that the three elastic constants characterizing splay, twist, and bend distortions of **n** are identical. Despite this fact, it correctly captures that equally charged defects repel while oppositely charged defects attract. Indeed, for $s_1 \cdot s_2 < 0$, the interaction force between defects, $F_{12} = -\nabla W_{12}$, is negative and results in their approach and annihilation; this has been well studied in flat liquid crystal cells [3–9]. By contrast, when $s_1 \cdot s_2 > 0$, $F_{12} > 0$ and the defects repel; they separate and maximize their distance, eventually reaching the boundaries of the cell [2].

The situation is very different in nematic droplets. In this case, when **n** is tangential at the bounding surface and splay is favored versus bend, there are two surface defects or boojums in the ground state; these are forced to coexist as a result of the topological constraints imposed by the Poincaré and Hopf theorem, which requires a total topological charge on the surface of the sphere equal to its Euler characteristic, χ [10]. Since for a sphere, $\chi = +2$, a total charge of $s_{\text{total}} = +2$ is required. As a result, each of the two defects has a charge of $s = +1$, which indicates the 2π rotation of **n** as we encircle the defect. This nematic configuration thus naturally provides the remarkable coexistence of equally charged defects a finite distance away from each other. Similar configurations also exist in nematic shells, where the liquid crystal is confined between two spherical surfaces. For these shells, when sufficiently thin, the ground state is populated with four $s = +\frac{1}{2}$ disclination lines that span the thickness of the shell. Nematic spheres thus provide unique opportunities to study the behavior of equally charged defects that would otherwise be impossible to study in flat space.

In this Rapid Communication, we take advantage of this and study for the first time coalescence of defects with similar topological charge. We use nematic shells with four $s = +\frac{1}{2}$ lines and analyze their coalescence after changing the boundary conditions for **n** at the outer surface from tangential to perpendicular. We observe that the four $s = +\frac{1}{2}$ disclinations coalesce by pairs into two single $s = +1$ boojums residing at the inner surface. Interestingly, the speed at which the two $s = +\frac{1}{2}$ disclinations move exhibits a maximum. By using numerical simulations, we show that this maximum results from the thickness inhomogeneity of our shells.

We study this transformation experimentally using double emulsion droplets produced in a glass-based microfluidic device [11,12] consisting of an inner aqueous droplet of radius a contained inside an outer liquid crystal droplet of radius R, which is in turn dispersed in an aqueous medium. The two aqueous fluids contain 1% wt of polyvinyl alcohol (PVA), which stabilizes the double emulsion and imposes tangential degenerate anchoring to the liquid crystal, 4-n-pentyl-4′-cyanobiphenyl (5CB). The resultant nematic shells have $R = 25$ μm and are heterogeneous in thickness as a result of buoyancy forces [11,13]; they are thinner at the top and thicker at the bottom and have an average thickness $h = R - a = 2.5$ μm. After fabrication, we place

*Present address: Laboratoire Charles Coulomb (L2C), UMR5221, Université Montpellier II, 34095 Montpellier, France.

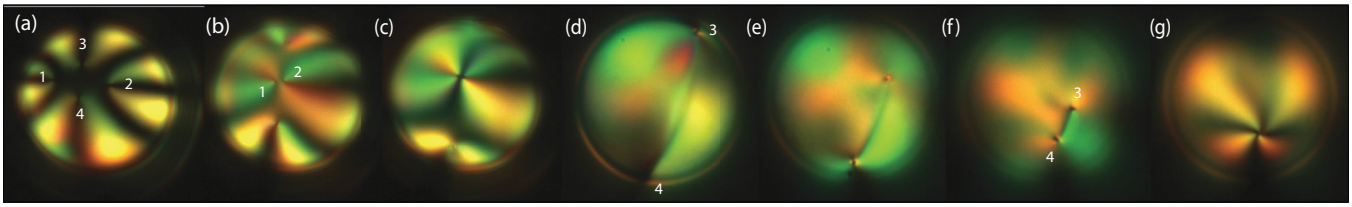

FIG. 1. (Color online) Cross-polarized images of a nematic shell after changing the boundary conditions at the outer surface from tangential to perpendicular. The different images correspond to different times after adding SDS: (a) 0 s, (b) 110 s, (c) 158 s, (d) 208 s, (e) 248 s, (f) 332 s, and (g) 790 s.

a drop of sample in a cuvette and change the molecular anchoring at the outer surface of the shells from tangential to perpendicular by adding a concentrated solution of sodium dodecyl sulfate (SDS). The final concentration of SDS in the cuvette is around 30 mM. The cuvette is sealed to prevent evaporation and located in an optical microscope under cross-polarizers.

Initially, when the boundary conditions are tangential at both spherical surfaces, the four $s = +\frac{1}{2}$ defect lines are localized at the top of the shell, as shown in Fig. 1(a). The equilibrium position observed results from the balance between the repulsion between disclinations of equal charge and the tendency of the lines to minimize their length. This configuration is altered when the SDS reaches the outer surface of the shell. At this point, defects 1 and 2 become connected with a new defect line and approach each other to coalesce into a single $s = +1$ defect; this is shown in Figs. 1(a)–1(c). Concomitantly, defects 3 and 4 move away from each other toward the equator of the shell. In this case, the defect line joining these defects is very obvious; it runs along the longer arc connecting the two defects, along the lower hemisphere, as shown in Figs. 1(b)–1(f). The line shrinks with time until defects 3 and 4 eventually also coalesce. The final state of the shell with these hybrid boundary conditions is characterized by the presence of two defects of charge $s = +1$ located on the inner sphere; they are an inner-droplet diameter away on different hemispheres, as shown in Figs. 1(c) and 1(g).

Imposing perpendicular anchoring at the outer surface while maintaining tangential anchoring at the inner surface forces the director to tilt inside the shell. As a result, there is a projection of **n** onto the inner surface that effectively results in a vector field on that surface. We show this using nails in Fig. 2, with the head of the nail indicating the tilt direction. In this situation, there is a π rotation of **n** across the line joining the two $s = +\frac{1}{2}$ defects resulting in formation of the defect line connecting both defects; this is shown in Fig. 2 also. On crossing this new line, **n** rotates by π. The line is thus a one-dimensional analog of a π wall. Its presence is energetically not favored and topologically not required. For this reason, the line shrinks while pulling the $s = +\frac{1}{2}$ pair together until the defects coalesce to form the final $s = +1$ defect.

We measure the time evolution of the two π lines, L_1 and L_2, joining the $s = +\frac{1}{2}$ defects by pairs. We observe that they shrink in a nonlinear way, as shown in Fig. 3(a). Therefore, the speed of the defects as they approach is not constant. Instead, the measured speed for the longest of the two π lines, v_2, exhibits a pronounced peak at a time corresponding to an angular separation of around $\theta_2 \approx \pi$, as shown in Fig. 3(b). This implies that the speed is maximum when the defects have reached the equatorial plane of the shell. The defects separate while accelerating, when they are in the upper hemisphere of the shell, and approach while decelerating, when they are in the lower hemisphere of the shell. Interestingly, the two defects participating in the coalescence process move at the same speed, in contrast to what happens when defects annihilate; in that case, since the defects have opposing charge, **n** has different contributions from splay and bend, resulting in different approaching speeds [6,8].

We also examine the coalescence of defects using Monte Carlo simulations of the nematic shells based on the Lebwohl-Lasher model for nematics, which has recently been used to study topological defects in concentric shells with tangential degenerate anchoring [13,14]. The model consists of rotors, representing a small volume of nematic with a well-defined local director, which are placed on the sites of a cubic lattice with spacing d. Nearest neighbors i and j interact via the potential $-\epsilon_{ij} P_2(\cos\beta)$, where $\epsilon_{ij} = \epsilon(>0)$ is an energy parameter, $P_2(x) = 3/2x^2 - 1/2$, and β is the angle between the neighboring rotors. Tangential anchoring at the boundaries can be obtained by using ghost particles pointing along the radial direction and setting $\epsilon_{ij} = -\epsilon(<0)$ for the nematic-boundary interaction. In our simulations, we set $R = 40d$ and $a = 25d$, with the inner sphere shifted $10d$ along the z direction to account for the buoyancy shift observed in the experiments. As for previous studies on nematic shells, we run our simulations at a single temperature $T^* = kT/\epsilon = 1.0$ [13,14], which is below the nematic-isotropic transition temperature $T^*_{NI} = 1.12$. We initially equilibrate the system with tangential anchoring at both surfaces and then change the nature of the ghost particles

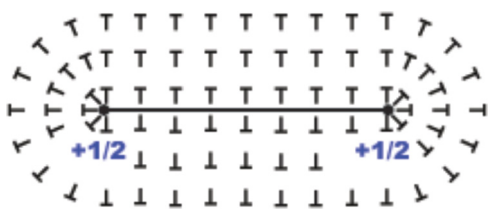

FIG. 2. (Color online) Schematic representation of the director field around two $s = +\frac{1}{2}$ defects on the inner spherical surface when the boundary conditions are tangential at that surface and perpendicular at the outer surface. The heads of the nails represent the tilt direction of **n** along the shell thickness. The different tilt across the line connecting the two $s = +\frac{1}{2}$ results in the formation of the observed π line that joins them.

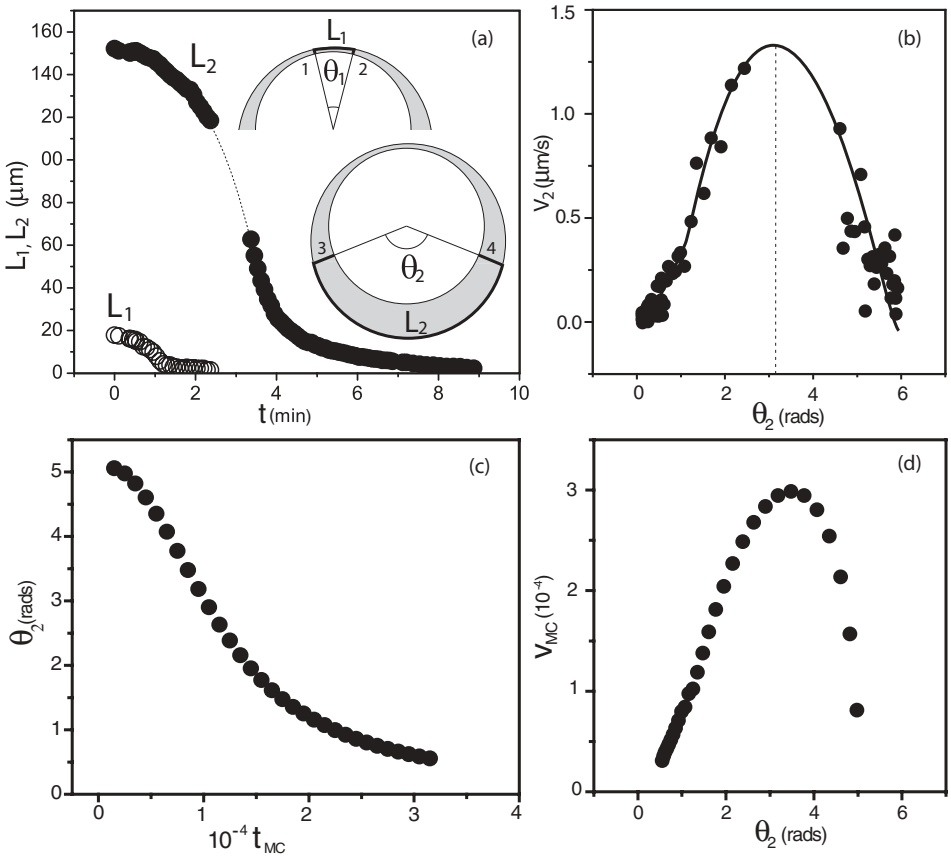

FIG. 3. Distance between defects 1 and 2 and between defects 3 and 4 as a function of time in (a) experiments and (c) simulations. Speed of defects 3 and 4 as a function of the angle between them in (b) experiments and (d) simulations.

at the outer surface by switching the sign of the interaction parameter to $\epsilon_{ij} = \epsilon(>0)$; this favors perpendicular anchoring at the outer surface. As for the experiments, the nature of the inner boundary is left unchanged. We use the method of Callan-Jones *et al.* to determine the local director field and Westin matrices to obtain the extent of local ordering [15].

When the anchoring is tangential at both inner and outer surfaces, the four $s = +\frac{1}{2}$ defects cluster near the top of the shell, consistent with the experimental results, as shown in Fig. 4(a). After changing the anchoring, a thin region at the outer surface rapidly disorders, as the molecules must rotate to fulfil the new boundary conditions for **n**. However, the director configuration inside the majority of the shell remains unchanged. Soon afterward, this disorder at the outer surface disappears, and two π lines appear on the outer surface, as shown in Fig. 4(b). The ends of these two lines are located roughly at the positions of the original $s = +\frac{1}{2}$ defects, with one line being much longer than the other. As the simulation progresses, the shorter line rapidly decays in length [Fig. 4(c)] while the longer of these lines gradually shrinks, bringing the two $s = +\frac{1}{2}$ defects to the lower hemisphere of the shell, as shown in Figs. 4(d) and 4(e). Interestingly, this π line does not start to move significantly towards the inner sphere right after it starts shrinking. Instead, it remains at the outer surface of the shell and only starts to peel away from the outer surface once it has significantly shrunk in length. Finally, the system reaches a new equilibrium state compliant with the new boundary conditions, consisting of two $s = +1$ boojums an inner-sphere diameter away from each other, as shown in Fig. 4(f). It is clear that the director field is tilted and that the nature of the two $s = +1$ boojums is quite different. The top defect is a half hyperbolic hedgehog whereas the bottom defect is a half radial hedgehog; this is consistent with experiments [16]. Despite being a stochastic rather than a dynamic technique,

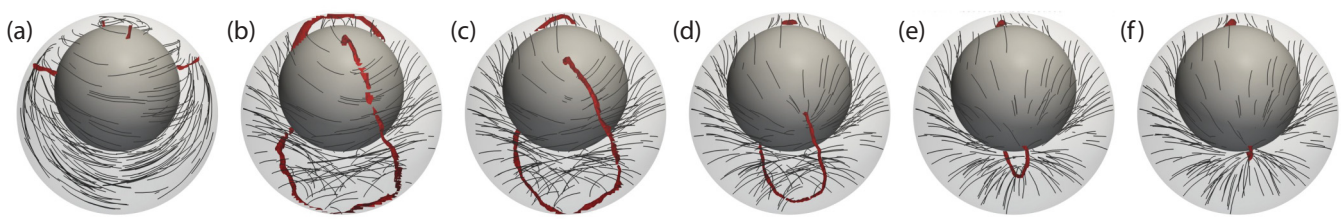

FIG. 4. (Color online) Simulated director field and defect lines along the process. In panel (a), the anchoring is tangential at both confining surfaces and the thick lines are the four $s = +\frac{1}{2}$ lines expected for this situation. Panel (b) corresponds to a shell with tangential and perpendicular boundary conditions on the inner and outer spheres, respectively. The two thick lines shown are π lines joining the $s = +\frac{1}{2}$ defects. Panels (c) and (d) are snapshots showing the evolution of the π lines. (f) Final equilibrium configuration with two $s = +1$ boojums on the inner sphere.

the overall evolution of the defect lines in the Monte Carlo simulations agrees very well with the experimental results.

We further analyze our simulation results by identifying the ends of the long π line and plot the angle connecting the two $s = +\frac{1}{2}$ defects as the simulation progresses in Fig. 3(c). From this angle, we obtain the speed, which is peaked at $\theta_2 \approx \pi$, as shown in Fig. 3(d). The simulations thus capture all features of the experimental dynamics very well.

To understand the presence of the maximum in speed, we consider the relevant forces in our problem. There is a repulsive elastic force between defects resulting from their equal charge: $F_1 = \frac{2\pi K s^2 h}{L}$, where L is the distance between disclinations. We adopt the one-constant approximation in writing this force, which is only important at very short distances. As a result, it does not play a major role during most of the transformation. There is also an attractive force associated with the π line joining the two $s = +\frac{1}{2}$ defects. This line tension pulls the two $s = +\frac{1}{2}$ defects together. We estimate this force using [7] $F_2 = -\pi k(1 + \ln \frac{h}{\pi l}) \approx -\pi k \ln \frac{h}{\pi l}$, where l is the anchoring extrapolation length, which is typically much smaller than h. Finally, there is a drag force opposing the motion [2]: $F_3 = -\frac{1}{4}\pi\gamma v h \ln \frac{3.6}{E_r}$, where γ is an average viscosity of the liquid crystal, v is the speed of the defects, and E_r is the Ericksen number, $E_r = \frac{\gamma v h}{k}$.

We balance F_2 and F_3 and obtain the shell-thickness dependence of the speed: $v \propto \frac{1}{h} \ln \frac{h}{\pi l}$. Since, in our shells, h depends on the zenithal angle $\theta = \pi - \theta_2/2$ as $h(\theta) \approx h(1 - \cos\theta)$, this balance naturally results in a peaked speed, suggesting that the observed maximum is due to the shell-thickness inhomogeneity. To test this, we perform additional simulations with concentric shells. We find that the maximum in speed disappears, confirming that indeed it results from the shell-thickness inhomogeneity.

The model, however, does not correctly capture the height of the peak observed experimentally. For typical values of the involved parameters, $K = 10^{-11}N$, $\gamma = 50cP$, and $l = 10$ nm, we find a speed at the peak of 10^3 μm/s, which is about three orders of magnitude larger than the value obtained experimentally, 1 μm/s. This discrepancy can be due to the details of how the molecular anchoring is changed in the experiment. It is known that the anchoring provided by SDS on 5CB progressively varies from tangential to perpendicular as a function of SDS concentration [17]. As a result, it is reasonable to think that while at the beginning of the process only a small number of SDS molecules have reached the outer surface, as time proceeds this number increases, progressively changing the tilt angle until full perpendicular alignment is achieved. Under these conditions, the line tension is expected to be weaker than that considered in our estimate of F_2 for some of the coalescence process. Indeed, we observe that the line only is clearly seen once the defects have reached the lower hemisphere of the shell. Detailed calculations are required to fully describe this effect and quantitatively describe the experimental results.

We have studied the coalescence process of $s = +\frac{1}{2}$ defects in the curved space of a nonuniform-thickness spherical shell by taking advantage of the presence of four of these defects in the ground state of the system. This has been achieved by changing the molecular anchoring at the outside boundary of the shell from tangential to perpendicular. The coalescence is driven by the presence of two π lines connecting the defects by pairs. We have found both experimentally and by simulation that the speed at which the $s = +\frac{1}{2}$ defects approach exhibits a peak that results from the thickness inhomogeneity of the shells. While defect annihilation in flat cells [8] and the effects of a change in the boundary conditions in drops and shells have been studied in the past [2,16,18–20], our study reports coalescence of equally charged defects to form a single defect with a larger topological charge. The essential role of curvature to achieve this might also be used to address other problems that are hard or impossible to address in flat space.

A.F-N. thanks the National Science Foundation (Career Award DMR-0847304) for support. T.L-L. thanks the European Marie Curie Program (IEF-236091) for support.

[1] J. P. Sethna, *Statistic Mechanics: Entropy, Order Parameters, and Complexity* (Oxford University Press, Oxford, 2006).
[2] M. Kleman and O. D. Lavrentovich, *Soft Matter Physics: An Introduction* (Springer-Verlag, New York, 2003).
[3] M. Svetec *et al.*, Eur. Phys. J. E **20**, 71 (2006).
[4] A. N. Pargellis *et al.*, Phys. Rev. A **46**, 7765 (1992).
[5] I. Chuang, B. Yurke, A. N. Pargellis, and N. Turok, Phys. Rev. E **47**, 3343 (1993).
[6] D. Svenŝek, and S. Žumer, Phys. Rev. E **66**, 021712 (2002).
[7] A. Bogi, P. Martinot-Lagarde, I. Dozov, and M. Nobili, Phys. Rev. Lett. **89**, 225501 (2002).
[8] C. Blanc, D. Svensek, S. Zumer, and M. Nobili, Phys. Rev. Lett. **95**, 097802 (2005).
[9] I. Dierking, O. Marshall, J. Wright, and N. Bulleid, Phys. Rev. E **71**, 061709 (2005).
[10] H. Poincaré, J. Math. Pures Appl. **1**, 167 (1885).
[11] A. Fernandez-Nieves, V. Vitelli, A. S. Utada, D. R. Link, M. Marquez, D. R. Nelson, and D. A. Weitz, Phys. Rev. Lett. **99**, 157801 (2007).
[12] A. S. Utada *et al.*, Science **308**, 537 (2005).
[13] M. A. Bates, G. Skaĉej, and Zannoni, Soft Matter **6**, 655 (2010).
[14] G. Skaĉej and C. Zannoni, Phys. Rev. Lett. **100**, 197802 (2008).
[15] A. C. Callan-Jones, R. A. Pelcovits, V. A. Slavin, S. Zhang, D. H. Laidlaw, and G. B. Loriot, Phys. Rev. E **74**, 061701 (2006).
[16] T. Lopez-Leon and A. Fernandez-Nieves, Phys. Rev. E **79**, 021707 (2009).
[17] J. M. Brake and N. L. Abbott, Langmuir **18**, 6101 (2002).
[18] G. E. Volovik and O. D. Lavrentovich, Sov. Phys. JETP **58**, 1159 (1983).
[19] O. O. Prishchepa, A. V. Shabanov, and V. Y. Zyrvanov, JETP Lett. **79**, 257 (2004).
[20] O. O. Prishchepa, A. V. Shabanov, and V. Y. Zyryanov, Phys. Rev. E **72**, 031712 (2005).